

Solid 226 nm laser pumped by a Nd:YAG laser for two-photon absorption detection of oxygen

Yi Zhang, Shaoyi Wang, Minghao Yu, Zhongqi Feng, and Dacheng Zhang*

Xidian University, School of Optoelectronic Engineering, Xi'an, China

Abstract. We present a solid 226 nm deep ultraviolet laser system pumped by a Nd:YAG laser. A diamond Raman laser with a 1485 nm wavelength was generated up to 2.53 mJ pumped by a 9.7 mJ 1064 nm laser, which is the highest pulse energy of a second Stokes diamond Raman laser pumped by a 1064 nm laser as we know. Then, the Raman laser is mixed with the frequency-quadrupled 1064 nm laser to produce the 226 nm laser. The maximum output pulse energy at 226 nm reaches 0.49 mJ. The overall conversion efficiency from 1064 to 226 nm is up to 1.14%, which is significantly higher than conventional optical parametric oscillator technology for the generation of 226 nm laser. The 226 nm laser system has been used in a laser-induced fluorescence (LIF) experiment of oxygen two-photon to demonstrate its potential for LIF measurements.

Keywords: Raman laser; deep ultraviolet; laser-induced fluorescence; sum-frequency; two-photon absorption.

Received Apr. 23, 2025; revised manuscript received Nov. 5, 2025; accepted for publication Nov. 10, 2025; published online Dec. 8, 2025.

© The Authors. Published by SPIE and CLP under a Creative Commons Attribution 4.0 International License. Distribution or reproduction of this work in whole or in part requires full attribution of the original publication, including its DOI.

[DOI: [10.1117/1.APN.5.1.016003](https://doi.org/10.1117/1.APN.5.1.016003)]

1 Introduction

Deep ultraviolet (DUV) lasers are attractive for many scientific and industrial applications, such as spectroscopy,^{1,2} laser fusion,^{3,4} biomedicine,^{5,6} optical communications,^{7,8} rapid disinfection or inactivation of bacteria, fungi, and viruses.^{9,10} In particular, a DUV laser with a 226 nm wavelength can resonantly excite the NO and oxygen molecules from their ground electronic state to an excited state. Then, the molecules can emit fluorescence, which can be used as planar laser-induced fluorescence (PLIF) and two-photon absorption laser-induced fluorescence (TALIF) to measure the spatial and temporal distributions of NO and oxygen molecules in hypersonic flows and combustion environments. It can be used to determine the flow rates and average temperatures and to study air lasing.^{11–16} Until now, the DUV laser has still mainly relied on cascaded nonlinear frequency conversion starting from a pulsed infrared solid-state laser.^{17–24} In these works, expanding the mature Nd:YAG lasers to new wavelengths by nonlinear frequency conversion technologies is perhaps more commercially attractive. In 2020, a 226 nm laser was generated by mixing a 393 nm laser from the second harmonic of the Ti:Sapphire laser with a 532 nm laser from the second harmonic of the distributed feedback diode

laser at 1064 nm using a BBO crystal. The maximum pulse energy at 226 nm was 3 mJ by mixing a 5 mJ 393 nm laser with a 25 mJ 532 nm laser.²¹ The same year, an optical parametric oscillator (OPO) pumped by a Nd:YAG laser was frequency doubled to 226 nm with a maximum pulse energy of 2 mJ.¹⁹ The OPO laser not only requires strict phase matching and a complex structure, but also the beam of OPOs cannot be transmitted over long distances due to its relatively poor quality of the output laser beam.^{25,26}

Raman frequency shift is another method to produce a new laser wavelength. A Raman laser has many merits, such as narrower free-running linewidth, freedom from phase-match in constraints, pulse length shortening, and even beam quality improvement through Raman beam cleanup.^{27,28} Chemical vapor deposition diamond (CVD-diamond) has garnered significant research interest as a Raman converter due to its larger Raman frequency shift (1332.3 cm^{-1}) compared with other Raman media. The most striking merits of diamond include a higher Raman gain coefficient (10 to $12 \text{ cm/GW}@1064 \text{ nm}$) and a higher thermal conductivity ($2200 \text{ W} \cdot \text{cm}^{-1} \cdot \text{K}^{-1}$). Its excellent thermal properties can dissipate any additional heat very well.²⁹ The large Raman shift of CVD-Diamond provides a good choice to generate $1.5 \mu\text{m}$ emission from the second Stokes shift pumped by the $1 \mu\text{m}$ Nd:YAG laser. In 2011, a 51% conversion efficiency from 1064 to 1485 nm was achieved using a

*Address all correspondence to Dacheng Zhang, dch.zhang@xidian.edu.cn

6.9-mm-long diamond pumped by a Nd:YAG laser with 3.2 W power at a repetition rate of 5 kHz.³⁰ In 2016, the maximum pulse energy at 1485 nm was 0.7 mJ pumped by a 4.4 mJ 1064 nm laser with a 30 ns pulse duration.³¹

In this work, we present a solid DUV nanosecond laser at 226 nm by combining a diamond Raman laser and sum-frequency generation (SFG) technology. A nanosecond diamond Raman laser emitting a second Stokes shift at 1485 nm pumped by a Nd:YAG laser was developed. Then, a 226 nm laser was obtained by mixing the second Stokes emission with the frequency-quadrupled Nd:YAG laser. To our knowledge, it is the first DUV laser at 226 nm generated by combining a diamond Raman laser with the SFG technology. The 226 nm laser has been used in an oxygen-TALIF experiment to test its ability for laser spectroscopy.

2 Experimental Setup

The experimental setup for 226 nm laser generation is shown in Fig. 1. The 226 nm laser was pumped by a linearly polarized Q-switched Nd:YAG laser (Dawa-300, Beamtch Optronics Co., Ltd., China) with a pulse duration of 9 ns and a repetition rate of 10 Hz at 1064 nm. The second harmonic generation of a 532 nm laser was generated from a 1064 nm laser by a KTP crystal with a size of 5(W) mm × 5(H) mm × 5(L) mm. The 532 nm laser was separated by a dichroic mirror DM1 (HR@532 nm/HT@1064 nm). Then, a 532 nm laser was injected into a BaB₂O₄ (BBO) crystal (BBO1) with a size of 5(W) mm × 5(H) mm × 5(L) mm to generate a 266 nm laser by frequency doubling again. The BBO1 was cut as a type-I crystal with the phase-matching angle of 47.6 deg. A CVD-diamond crystal (Element Six, UK) with a size of 2(W) mm × 2(H) mm × 7(L) mm was used as a Raman medium. The residual 1064 nm laser after generation a 532 nm laser was used to pump the CVD-diamond crystal to generate a second Stokes shift laser at 1485 nm. The crystal was cut for propagation along the $\langle 110 \rangle$ axis and coated with anti-reflection films of 1064, 1240, and 1485 nm at both ends. The pulse energy of the pump laser can be varied using the half-wave plate HWP2 and polarization beam splitter (PBS). The second half-wave plate HWP2

was used to align the polarization axis of the pump laser to the $\langle 111 \rangle$ axis of the diamond to maximize Raman gain.^{29,32}

The diameter of the pump laser was reduced to 3 mm using a telescope system composed of a pair of lenses with focus lengths $f = 200$ mm and $f = -75$ mm. Then, an aperture was used to reduce the diameter of the pump laser to 1.8 mm. The aperture can improve the beam quality of the pump laser by selecting the central part of the pump beam. The diamond Raman laser cavity is a flat-flat cavity structure composed of an input coupler mirror and an output coupler mirror. The input coupler mirror of the cavity was highly transmissive (HT) at 1064 nm and highly reflective (HR) at 1240 and 1485 nm. The output coupler mirror of the cavity was highly reflective at 1064 and 1240 nm and partially transmissive ($T = 45\%$) at 1485 nm, providing optimal output coupling. The 266 nm laser was collimated with the 1485 nm laser by a dichroic mirror DM6 (HR@266 nm/HT@1485 nm). Finally, the 266 nm laser beam and 1485 nm laser beam are both injected into a BBO crystal (BBO2) with a size of 5(W) mm × 5(H) mm × 10(L) mm to generate the 226 nm pulse by sum-frequency generation. The BBO2 was cut as a type-I crystal with a phase-matching angle of 42.7 deg. The 226 nm laser was separated by a JGS1 prism from other wavelengths behind the BBO2 crystal due to the absence of an ideal dichroic mirror for 266 and 226 nm lasers.

3 Parameters of the DUV Laser

The output parameters of the DUV laser such as pulse energy, duration, and wavelength were studied in this work. The pulse energy of the laser was measured by a laser energy meter (LabMax-TOP with EM USB J-10MB-HE detector, Coherent Inc.). The variation of the pulse energy of the Raman laser with its cavity length was studied. The output pulse energies and conversion efficiencies of the second Stokes Raman laser pumped by different pulse energy of a 1064 nm laser at three different cavity lengths are shown in Fig. 2. To avoid the damage of input coupler (IC) mirror and diamond, the maximum pump energy was limited to 10 mJ. At a 19 mm cavity length, the 1485 nm laser produced an output energy of 2.53 mJ with a 9.7 mJ 1064 nm pump laser, corresponding to a conversion efficiency of 26.1%. The maximum conversion efficiency of 27.0% was

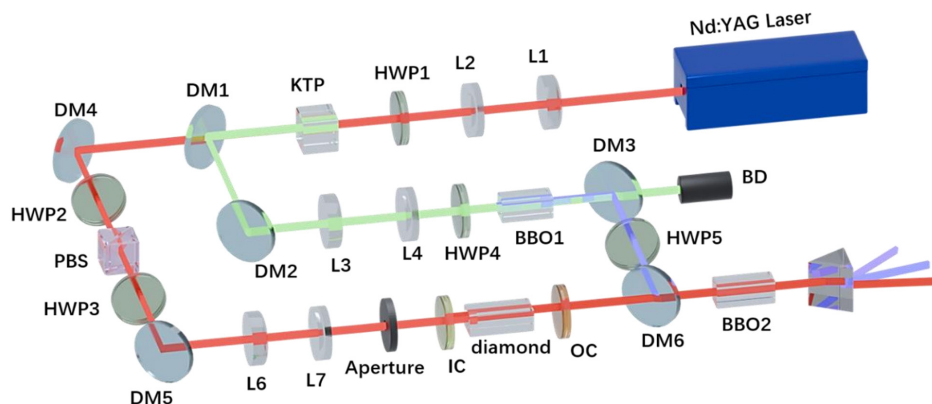


Fig. 1 Schematic of the 226 nm laser system layout. HWP, half-wave plate; DM1, DM2, HR@532 nm/HT@1064 nm dichroic mirrors; DM4, DM5, HR@1064 nm reflectors; DM3, HR@266 nm/HT@532 nm dichroic mirror; DM6, HR@266 nm/HT@1485 nm dichroic mirror; PBS, polarization beam splitter; IC, input coupler mirror; OC, output coupler mirror.

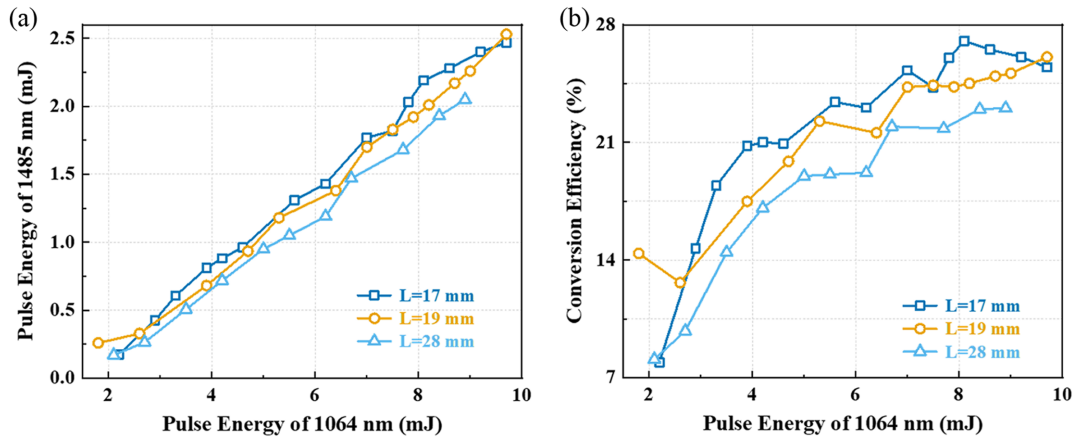


Fig. 2 (a) Output pulse energy and (b) conversion efficiency at the second Stokes emission versus pump energy for three cavity lengths of 17, 19, and 28 mm.

achieved with a 17 mm cavity and an 8.7 mJ 1064 nm pump laser. With the increase in the pump energy from 8.1 to 9.7 mJ, the conversion efficiency decreased from 27.0% to 25.5%. The pulse energy of the Raman laser increased linearly with pump energy for cavity lengths of 19 and 28 mm, but conversion efficiency saturation was observed for the cavity length of 17 mm. It can also be found that the conversion efficiency is higher for short cavities such as 17 and 19 mm compared with longer cavities such as 28 mm. The longer cavities lead to the higher diffraction losses, which reduce the Raman laser gain and improve the laser threshold. By contrast, shorter cavities allow more gain cycles within the same time frame and result in a smaller diameter of the second Stokes beam. It means the conversion efficiency in a shorter resonator reaches the saturation faster. To the best of our knowledge, it is the highest pulse energy of the second Stokes diamond Raman laser pumped by a Nd:YAG laser at 1064 nm.

The pulse duration was measured by a photodiode detector (DET10A2, Thorlabs). As shown in Fig. 3(a), the pulse duration of the second Stokes laser is 5.4 ns, which is shorter than the 8.7 ns pulse duration of the pump laser. Stimulated Raman scattering frequency conversion leads to pulse compression of the Stokes components. The Raman generation process initiates only when the leading edge of the pump pulse exceeds the threshold intensity, with subsequent rapid energy depletion during peak pump intensity confining the Raman output primarily to the pulse front region.³⁰ The insets in Figs. 3(b) and 3(c) shows the beam profiles of pump and Raman lasers measured by a CCD camera (MER-134-93U3C, DaHeng Imaging). It can be found that the beam quality was significantly improved by the diamond Raman laser, which is beneficial to generate a DUV laser with high efficiency.

The influence of second-order Raman laser energy on the 226 nm deep ultraviolet laser energy was studied. The spectra

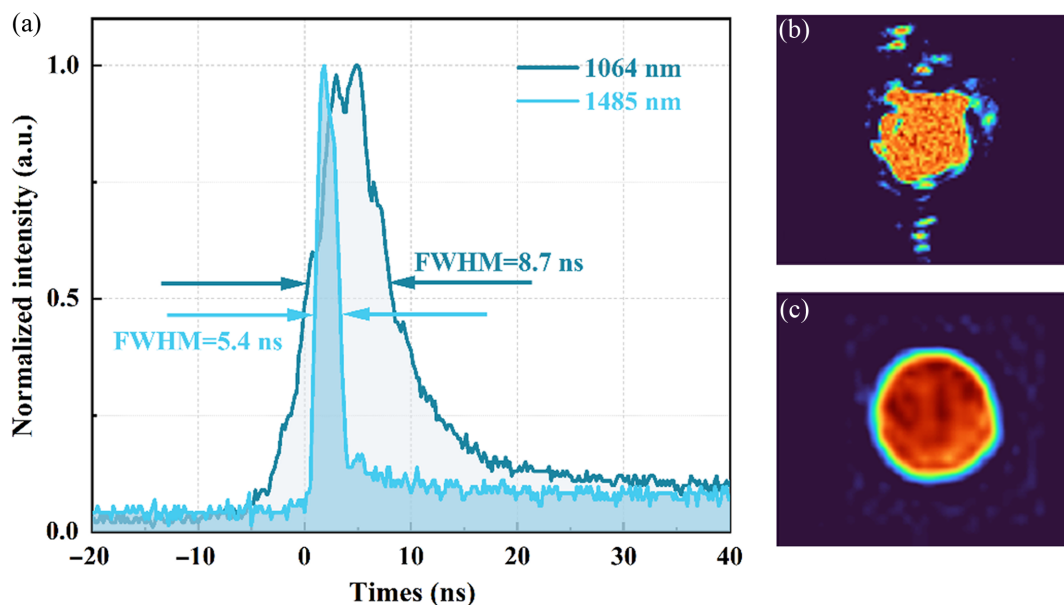


Fig. 3 (a) Pulse shapes of the pump laser before entering the Raman resonator and the second Stokes emission at a cavity length of 19 mm. (b) Input and (c) Raman beam profiles.

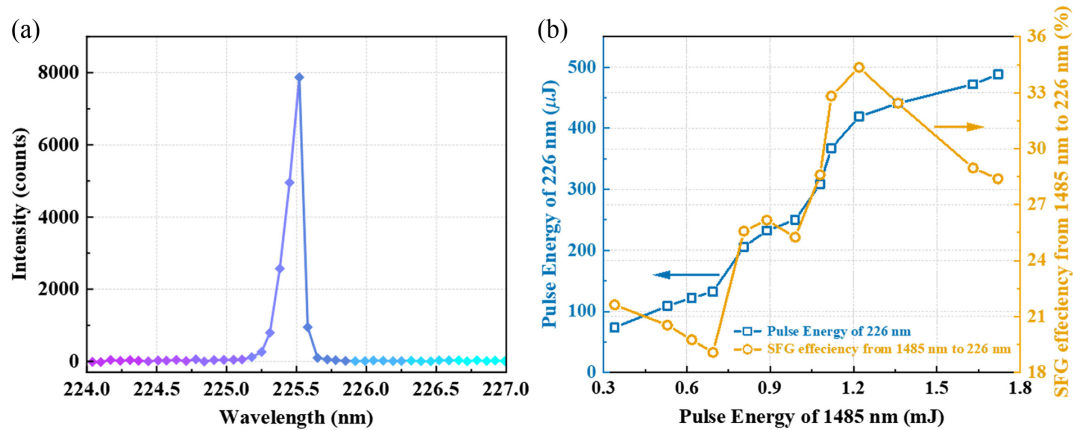


Fig. 4 (a) Spectrum of the 226 nm laser; (b) output energy and conversion efficiency of SFG from 1485 to 226 nm under the 4.3 mJ energy of 266 nm laser.

of the 226 nm laser were measured using a fiber spectrometer (AvaSpec-ULS2048, Avantes) with a spectral resolution of 0.08 nm over the range of 220 to 335 nm. To accurately measure the pulse energy of the 226 nm laser, a JGS1 prism was used to separate the 226 nm laser from the residual 266 nm laser. However, the transmissivity of the prism is only 68% for the DUV laser and the real pulse energy of 226 nm laser should be corrected by the transmissivity. When the pulse energy of the 266 nm was fixed at 4.30 mJ, the pulse energy of 226 nm laser versus the 1485 nm pumped laser was measured, as shown in Fig. 4(b). It can be found that the maximum pulse energy of 226 nm is 0.49 mJ produced by combining a 1.72 mJ 1485 nm laser with a 4.3 mJ 266 nm laser. The corresponding conversion efficiency from 1485 nm laser to 226 nm laser is 28.4%. The maximum conversion efficiency is 34.4% when the pulse energy of 1485 nm is 1.22 mJ. The decrease in the conversion efficiency for the more than 1.22 mJ 1485 nm laser should be attributed to the mismatch of the beam spots. The spot size of the 1485 nm laser is larger than that of the 266 nm laser in the BBO2 crystal, which leads to only part of the 1485 nm photons can be used to generate 226 nm laser. With the increasing of the pulse energy of the 1485 nm laser, more photons of 1485 nm outside the 266 nm beam were wasted. It should be pointed out that the BBO crystals used in this work are not exactly designed for 226 nm generation but for 220 nm, which

could introduce some walk-off. Thus, the conversion efficiency from 1485 nm laser to 226 nm laser could be improved further by a specially designed BBO crystal. Due to the conversion efficiency from 1064 to 266 nm, which was 10%, the pump energy of 1064 nm used for the generation of a 4.3 mJ 226 nm laser was about 43 mJ. The pulse energy used for pumping Raman laser is residual 1064 nm laser after first stage frequency doubling. Thus, the overall 1064 nm-to-226 nm conversion efficiency for generation 0.49 mJ 226 nm laser is up to 1.14%, which is nearly three folds than a conventional OPO technology in this wavelength.

4 Two-Photon Fluorescence Experiments

To test the ability of the DUV laser for fluorescence spectroscopy, an oxygen TALIF experiment was performed in ambient air. The experimental setup for oxygen TALIF is depicted in Fig. 5(a). A Nd:YAG laser emitting 1064 nm was used to produce plasma in air. The laser pulse with 56 mJ pulse energy was focused by a quartz lens with a 90 mm focal length. Then, the 226 nm laser with 100 μJ pulse energy was focused by a quartz lens with a 60 mm focal length to irradiate the plasma. The oxygen atom can be resonantly excited by two-photon and then emit 845 nm fluorescence schematically described in Fig. 5(b). The fluorescence was detected by a photomultiplier (PMT),

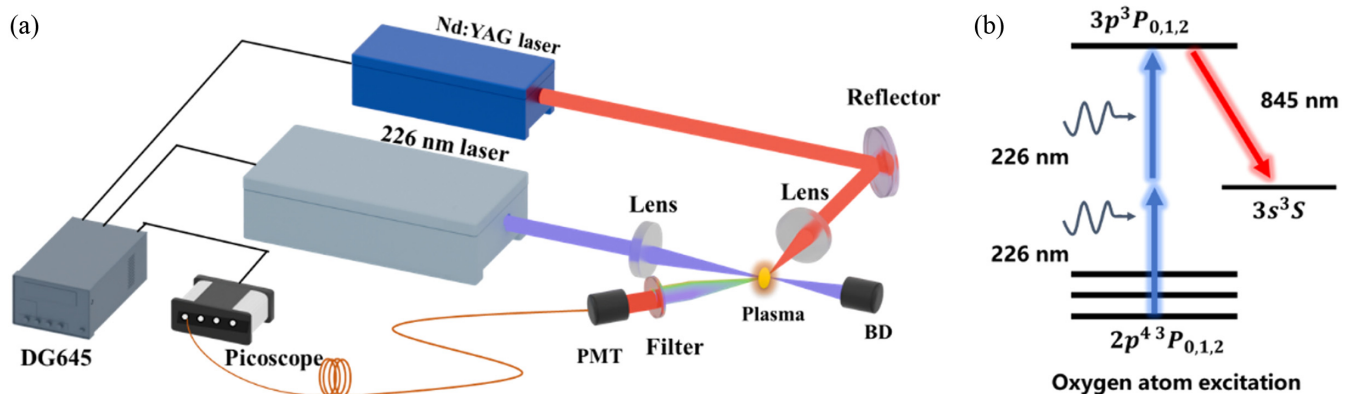


Fig. 5 (a) Schematic of the experimental setup for laser-induced fluorescence of oxygen. (b) The energy level diagram of oxygen atom.

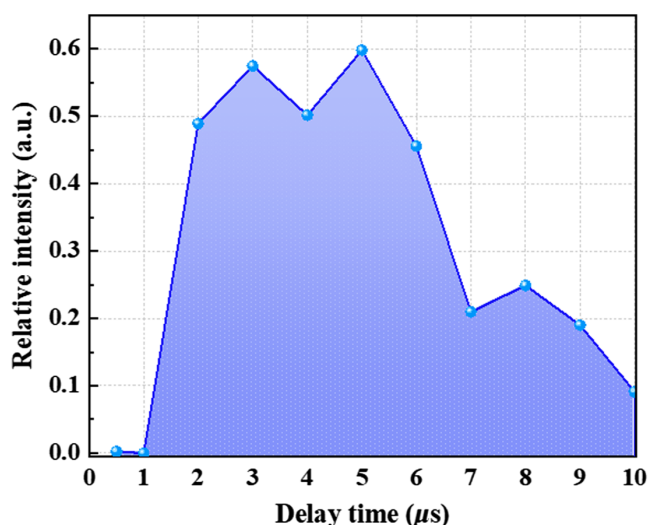


Fig. 6 Evolution of the fluorescence of oxygen with delay time between the Nd:YAG laser and the 226 nm laser.

H10722-20, Hamamatsu, Japan). To avoid the interference from plasma emission, a narrow-band filter (FB850-40-1, Thorlabs, USA) and was mounted on the window of the PMT. The PMT operates within a wavelength response range of 230 to 920 nm. The signal of PMT was recorded by an acquisition card (PicoScope 6424E, Pico Technology, UK). The delay time among the Nd:YAG laser, the 226 nm laser and the data acquisition card was controlled by a digital signal delay generator (Stanford Research Systems, DG645). In experiments, the delay time between the Nd:YAG laser and 226 nm laser can be adjusted to study the evolution of oxygen atoms in plasma. The acquisition card was triggered earlier 280 ns than 226 nm laser arrival to acquire the fluorescence signal as possible.

The pure fluorescence signal excited by a 226 nm laser was acquired by subtracting the plasma emission without the 226 nm laser. The averaged results from 100 pulses were measured to reduce the signal fluctuation induced by the fluctuation of laser pulse energy. Figure 6 shows the evolution of the fluorescence with the delay time between the ablation laser and the re-excited laser. It can be found that the intensity of fluorescence from oxygen increases very fast within 2 μ s and maintains nearly 10 μ s, which is consistent with the evolution of laser-induced plasma. It means that the laser has been used to detect the oxygen atoms by two-photon excitation successfully.

5 Conclusion

A nanosecond DUV laser source at 226 nm using the SFG between the diamond Raman laser and fourth harmonic generation based on the Nd:YAG laser was first demonstrated in this work. The diamond Raman laser at 1485 nm pumped by a Nd:YAG laser was designed and the conversion efficiency can be up to 27%. The maximum pulse energy of 1485 nm laser is 2.53 mJ, which is the highest pulse energy for a second Stokes diamond Raman laser pumped by a Nd:YAG laser. Then, the 226 nm laser was generated by the sum-frequency of the frequency-quadrupled 1064 nm laser and the second Stokes diamond Raman laser. The maximum pulse energy of the 226 nm laser is 0.49 mJ. The solid 226 nm laser has been used as a laser source

in the TALIF experiment, and the fluorescence of oxygen atoms in plasma by two-photon absorption has been successfully observed. It can also be used as a laser source for PLIF experiments of nitric oxide. Although the wavelength of the 226 nm laser in this work cannot be tunable, the abilities in spectroscopy analysis of oxygen have been demonstrated. In future, a Fabry-Prot etalon or other dispersion elements can be inserted to the cavity of Nd:YAG, and the laser can be tunable nearly 100 GHz around 226 nm for precision spectroscopy. If a Yb^{3+} doped media laser is used instead of the Nd:YAG as the pump laser, a more widely tunable range can be achieved,^{33,34} which could meet more laser spectroscopy applications.

Disclosures

No conflicts of interest, financial or otherwise, are declared by the authors.

Code and Data Availability

The code and data that support the findings of this study are available from the corresponding author upon reasonable request.

Acknowledgments

This work was supported by the National Natural Science Foundation of China (Grant Nos. U2032136 and U2241288) and the Shaanxi Fundamental Science Research Project for Mathematics and Physics (Grant No. 23JSY012).

References

1. R. K. Altmann et al., "High-precision Ramsey-comb spectroscopy at deep ultraviolet wavelengths," *Phys. Rev. Lett.* **117**, 173201 (2016).
2. Z. Y. Xu et al., "Advances in deep ultraviolet laser based high-resolution photoemission spectroscopy," *Front. Inf. Technol. Electron. Eng.* **20**, 885–913 (2019).
3. R. Betti and O. A. Hurricane, "Inertial-confinement fusion with lasers," *Nat. Phys.* **12**, 435–448 (2016).
4. S. P. Obenschain et al., "Direct drive with the argon fluoride laser as a path to high fusion gain with sub-megajoule laser energy," *Philos. Trans. R. Soc. A: Math. Phys. Eng. Sci.* **378**, 2020031 (2020).
5. Q. Fu et al., "High-power, high-efficiency, all-fiberized-laser-pumped, 260-nm, deep-UV laser for bacterial deactivation," *Opt. Express* **29**, 42485–42494 (2021).
6. Y. Kumamoto et al., "Deep-ultraviolet biomolecular imaging and analysis," *Adv. Opt. Mater.* **7**, 1801099 (2019).
7. R. J. Drost and B. M. Sadler, "Survey of ultraviolet non-line-of-sight communications," *Semicond. Sci. Technol.* **29**, 084006 (2014).
8. D. M. Maclure et al., "Hundred-meter Gb/s deep ultraviolet wireless communications using AlGaIn micro-LEDs," *Opt. Express* **30**, 46811–46821 (2022).
9. F. Chiappa et al., "The efficacy of ultraviolet light-emitting technology against coronaviruses: a systematic review," *J. Hosp. Infect.* **114**, 63–78 (2021).
10. I. Mehta et al., "UV disinfection robots: a review," *Rob. Auton. Syst.* **161**, 104332 (2023).
11. B. F. Bathel et al., "Velocity profile measurements in hypersonic flows using sequentially imaged fluorescence-based molecular tagging," *AIAA J.* **49**, 1883–1896 (2011).
12. B. S. Leonov et al., "High-speed planar laser-induced fluorescence investigation of nitric oxide generated by hypersonic Mach

- reflections for computational fluid dynamics validation,” *Phys Fluids* (1994) **35**, 066102 (2023).
13. D. J. Bamford et al., “Characterization of arcjet flows using laser-induced fluorescence,” *J. Thermophys. Heat Transf.* **9**, 26–33 (1995).
 14. C. T. Johansen et al., “Simultaneous nitric oxide/atomic oxygen laser-induced fluorescence in an arcjet facility,” *J. Thermophys. Heat Transf.* **30**, 912–918 (2016).
 15. A. Dogariu et al., “High-gain backward lasing in air,” *Science* **331**, 442–445 (2011).
 16. A. Laurain et al., “Low-threshold bidirectional air lasing,” *Phys. Rev. Lett.* **113**, 253901 (2014).
 17. P. Koch et al., “Single-mode deep-UV light source at 191.7 nm by seventh-harmonic generation of a high-power, Q-switched, injection-locked nm Nd:YVO4 laser,” *Appl. Opt.* **55**, 1871–1877 (2016).
 18. T. Nakazato et al., “Development of high coherence, 200 mW, 193 nm solid-state laser at 6 kHz,” *Proc. SPIE* **9342**, 93420P (2015).
 19. T. Jiang et al., “Single-frequency laser pumped optical parametric oscillator at 226 nm,” *Laser Phys.* **30**, 015801 (2020).
 20. B. Willenberg et al., “High-power picosecond deep-UV source via group velocity matched frequency conversion,” *Optica* **7**, 485–491 (2020).
 21. S. Dai et al., “Tunable narrow-linewidth 226 nm laser for hypersonic flow velocimetry,” *Opt. Lett.* **45**, 2291–2294 (2020).
 22. K. Le Corre et al., “Watt-level deep-UV subnanosecond laser system based on Nd-doped fiber at 229 nm,” *Opt. Lett.* **48**, 1276–1279 (2023).
 23. Z. T. Zhang et al., “High-power, narrow linewidth solid-state deep ultraviolet laser generation at 193 nm by frequency mixing in LBO crystals,” *Adv. Photonics Nexus* **3**, 026012 (2024).
 24. K. L. Corre et al., “Linearly-polarized pulsed Nd-doped fiber MOPA at 905 nm and frequency conversion to deep-UV at 226 nm,” *Opt. Express* **29**, 4240–4248 (2021).
 25. X.-L. Dong et al., “High-power 1.5 and 3.4 μm intracavity KTA OPO driven by a diode-pumped Q-switched Nd:YAG laser,” *Opt. Commun.* **282**, 1668–1670 (2009).
 26. M. S. Webb et al., “High-average-power KTiOAsO4 optical parametric oscillator,” *Opt. Lett.* **23**, 1161–1163 (1998).
 27. H. M. Pask, “The design and operation of solid-state Raman lasers,” *Prog. Quantum Electron.* **27**, 3–56 (2003).
 28. S. Singh et al., “Light correcting light with nonlinear optics,” *Adv. Photonics* **6**, 026003 (2024).
 29. R. P. Mildren et al., “Diamond Raman laser design and performance,” in *Optical Engineering of Diamond*, R. P. Mildren and J. R. Rabreau, Eds., pp. 239–276 (2013).
 30. A. Sabella et al., “Efficient conversion of a 1.064 μm Nd:YAG laser to the eye-safe region using a diamond Raman laser,” *Opt. Express* **19**, 23554–23560 (2011).
 31. V. P. Pashinin et al., “External-cavity diamond Raman laser performance at 1240 nm and 1485 nm wavelengths with high pulse energy,” *Laser Phys. Lett.* **13**, 065001 (2016).
 32. A. Sabella et al., “1240 nm diamond Raman laser operating near the quantum limit,” *Opt. Lett.* **35**, 3874–3876 (2010).
 33. L. Zhao et al., “Wavelength-tunable ultrafast vortex Yb:KGW laser,” *Opt. Laser Technol.* **184**, 112428 (2025).
 34. B. Jiang et al., “Simultaneous ultraviolet, visible, and near-infrared continuous-wave lasing in a rare-earth-doped microcavity,” *Adv. Photonics* **4**, 046003 (2022).

Dacheng Zhang is a professor in the School of Optoelectronic Engineering at the Xi'dian University. His recent work focuses on laser spectroscopy and laser technology, especially developing new laser sources for laser spectroscopy, such as portable high-peak power lasers and ultra-narrow linewidth nanosecond tunable lasers. He has published over 100 papers in peer-reviewed journals including *Ultrafast Science*, *Optics Express*, and *Spectrochimica Acta Part B*, and has been granted 15 invention patents.

Biographies of the other authors are not available.